*Progress In Electromagnetics Research C, Vol. 109, 187–203, 2021*

# Innovative Microwave Design of Frequency-Independent Passive Phase Shifter with LCL-Network and Bandpass NGD Circuit

**Jamel Nebhen[1, *] and Blaise Ravelo[2]**

**Abstract**—The present paper develops an application of the bandpass (BP) negative group delay (NGD) circuit for the design of an independent frequency phase shifter (PS). The design principle of the innovative PS is constituted by an inductor-capacitor-inductor (LCL) T-shape passive cell in cascade with RLC-network series-based BP NGD circuits. The $S$-matrix analytical model of the LCL-NGD PS is established in function of the circuit elements. Then, the design equations of the PS elements in the function of the expected PS value and center frequency are formulated. The NGD PS topology is validated with a comparison between the calculated and simulated results of phase, transmission coefficient, and reflection coefficients. As expected, a very good correlation between the analytical model and the simulation is confirmed by the obtained results. It is found that the LCL-NGD PS presents an outstandingly flat phase shift of $-120° \pm 5°$ with 1.2 GHz center frequency. The LCL-NGD PS operates with about 18% relative bandwidth. The PS reflection coefficient presents a magnitude flatness around $-3 \pm 1.5$ dB. Moreover, the reflection coefficient is kept better than $-15$ dB. The sensitivity of the LCL-NGD PS performances over the NGD circuit element $\pm 5\%$ relative variation is studied. It is found how the PS value and center frequency change with the R, L, and C components of the NGD circuit.

## 1. INTRODUCTION

Nowadays, the unfamiliar negative group delay (NGD) remains one of the most intriguing functions ever found in electronics engineering [1, 2]. Therefore, more didactic research works [1–18] are necessary to highlight the meaning and application of this particularly unfamiliar NGD function.

A bibliographic study enables us to state that the NGD effect was initially observed with the optical signal propagating through dispersive medium presenting negative refractive group index (NRI), $n_g(\omega) < 0$ [1, 2], which depends on the angular frequency, $\omega$. Indeed, the sign of group velocity $v_g(\omega)$ is the same as the group index one based on the analytical definition:

$$v_g(\omega) = \frac{c}{n_g(\omega)} < 0, \tag{1}$$

where $c$ is the speed of light in the vacuum. The corresponding group delay (GD) should also become negative for the medium having a physical length, $d$:

$$GD(\omega) = \frac{d}{v_g(\omega)}. \tag{2}$$

Because of its counterintuitive aspect, the NGD effect was fascinating for electronic design engineering researchers with NRI metamaterial structures [3–6]. However, the metamaterial microwave circuits are usually implemented with periodical structures [3–6]. Different topologies of RC-network lumped and distributed circuits exhibiting NGD effect were investigated [7–10]. To overcome the

*Received 2 January 2021, Accepted 29 January 2021, Scheduled 7 February 2021*
* Corresponding author: Jamel Nebhen (j.nebhen@psau.edu.sa).
[1] Prince Sattam bin Abdulaziz University, College of Computer Engineering and Sciences, P. O. Box 151, Alkharj 11942, Saudi Arabia. [2] Nanjing University of Information Science & Technology (NUIST), Nanjing, Jiangsu 210044, China.

inherent loss effects found with microwave NGD structures [3–6], active circuits with NGD effect were designed [11–14]. It was theoretically and experimentally demonstrated that the NGD effect enables the generation of output signal waveforms which superseded the input signal waveforms [7–9]. Therefore, the NGD effect is not in contradiction with the causality principle [7].

In last five years, many research works have been particularly focused on the design of compact and low attenuation NGD microwave circuits [15–17]. Different topologies of microwave NGD passive circuits implemented with a transmission line (TL) element were proposed [15–17]. The democratization of the NGD microwave circuit design was more and more initiated with the feasibility of various aspects regularly found with classical RF/microwave functions (filter, amplifier, power combiner, ...) as the tunable [16] and dual-band [17] NGD devices. Despite this progressive development of NGD circuit design, non-specialist RF/microwave engineers are curiously wondering about the meaning of the NGD effect. To answer such curiosity, a simple explanation based on the analogy between the filter and NGD functions was initiated in [18]. The concept of the bandpass (BP) NGD function which enables the classification of most of NGD microwave circuits as proposed in [3–6, 11–18] was introduced.

Behind the design research, the exploitability of the NGD function in microwave engineering requires further research work. Tentative NGD applications were proposed for the compensation of oscillators, filters, and communication systems [19], enhancement of feedforward amplifiers [20, 21], realization of non-Foster reactive elements [22], reconfigurable series feed network for squint-free antenna beamforming [23, 24], and GD compensation [25–27]. For the last case of application, the active NGD circuits were exploited to realize the compensation. In the present paper, we develop a potential application of the BP NGD function for the design of an independent frequency phase shifter (PS) with a fully passive circuit. Different from the positive GD (PGD) compensation principle proposed in [25, 26], instead of TL, the present study is innovatively based on the consideration of an LCL-lumped network associated with an RLC-series resonance passive NGD cell.

To highlight the investigation of the innovative PS circuit, the proposed paper is organized into four main sections as follows:

- Section 2 is focused on the design principle of the PGD-NGD PS. The analysis method of the unfamiliar BP NGD circuit and its main specifications will be defined. The elementary definitions necessary for the analysis of the PS will be introduced.
- The theory of the PS circuit implemented with a passive RLC-network will be explored in Section 3. The analytical study will be performed via the NGD circuit modeling and the modeling of the PGD circuit constituted by an LCL T-topology of the passive circuit. Then, the $S$-matrix model and design equation of the LCL-NGD PS will be explored.
- Section 3 is focused on the validation of the independent frequency PS response. The comparative results from the theoretical model and simulation from a commercial tool will be discussed.
- Finally, Section 4 concludes the paper with a synthetically summary.

## 2. DESIGN PRINCIPLE OF THE INNOVATIVE NGD PHASE SHIFTER (PS)

The present section introduces the analytical principle illustrating how to design an LCL-NGD PS. The theoretical $S$-parameter model will be established. The synthesis design equation to the desired PS value and the expected operation frequency are introduced.

### 2.1. $S$-Matrix Description of the PGD-NGD PS Topology

Similar to all classical microwave circuits, the present study is based on the consideration of a two-port $S$-matrix to represent the analytically equivalent model. The proposed independent frequency PS is built with the cascade combination of PGD and NGD circuits as illustrated in Fig. 1. By denoting the input signal, $V_{in}$, and the reference impedance, $R_0$, we assume the analytical general models of PGD, NGD, and both combined $S$-matrices by:

$$[S_{PGD}(j\omega)] = \begin{bmatrix} S_{11PGD}(j\omega) & S_{21PGD}(j\omega) \\ S_{21PGD}(j\omega) & S_{11PGD}(j\omega) \end{bmatrix}, \tag{3}$$

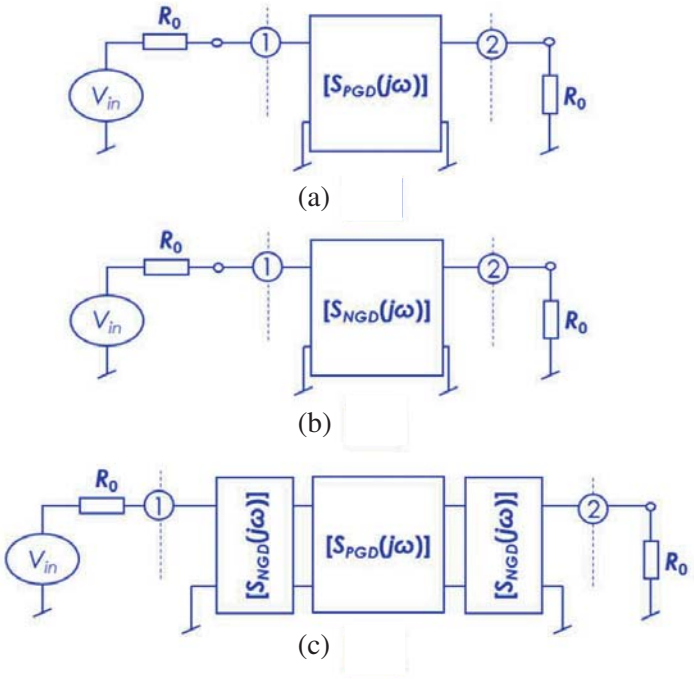


**Figure 1.** Block diagrams of (a) PGD, (b) NGD, and (c) PGD-NGD PS $S$-parameters.

$$[S_{NGD}(j\omega)] = \begin{bmatrix} S_{11NGD}(j\omega) & S_{21NGD}(j\omega) \\ S_{21NGD}(j\omega) & S_{11NGD}(j\omega) \end{bmatrix}, \tag{4}$$

$$[S_{PS}(j\omega)] = [S_{PGD-NGD}(j\omega)] = \begin{bmatrix} S_{11PGD-NGD}(j\omega) & S_{21PGD-NGD}(j\omega) \\ S_{21PGD-NGD}(j\omega) & S_{11PGD-NGD}(j\omega) \end{bmatrix}. \tag{5}$$

It is noteworthy that the considered PGD, NGD, and PS circuits are assumed as a passive and symmetrical system.

The $S$-matrix models are the building blocks of the analytical investigation of the proposed innovative PS. The next parts of the paper will exploit these $S$-matrix elements to define each parameter of the characterization.

### 2.2. Elementary Definitions for the PS Frequency Response Analyses

The frequency responses of the PGD and NGD circuits depend on the magnitude, phase, and GD exploration. We can recall in the present section the analytical definitions of these parameters. The magnitudes of the reflection and transmission coefficients are denoted by:

$$\begin{cases} S_{11x}(\omega) = |S_{11x}(j\omega)| \\ S_{21x}(\omega) = |S_{21x}(j\omega)| \end{cases}, \tag{6}$$

with subscript $x = \{PGD,\ NGD,\ PGD\text{-}NGD\}$. The associated transmission phase is given by:

$$\phi_x(\omega) = \arg\left[S_{21x}(j\omega)\right]. \tag{7}$$

The corresponding GD is defined as:

$$GD_x(\omega) = \frac{-\partial\phi_x(\omega)}{\partial\omega}. \tag{8}$$

Knowing these definitions, we can elaborate in the following subsections the analytical investigation on the PGD and NGD function under study.

### 2.3. PS Transmission Coefficient Approximation with the Interstage Matching of PGD and NGD Circuits

The interstage matching between the PGD and NGD circuit is formulated by the condition on the reflection coefficient in the NGD frequency band:

$$\begin{cases} S_{11PGD}(\omega) \ll 1 \\ S_{11NGD}(\omega) \ll 1 \end{cases}. \tag{9}$$

Under this condition, the PS transmission coefficient can be approximated by:

$$S_{21PGD\text{-}NGD}(j\omega) \approx S_{21NGD}(j\omega) \cdot S_{21PGD}(j\omega) \cdot S_{21NGD}(j\omega). \tag{10}$$

The phase of the PS diagram shown in Fig. 1(c) can be written as:

$$\phi_{PS}(\omega) \approx \phi_{NGD}(\omega) + \phi_{PGD}(\omega) + \phi_{NGD}(\omega) = 2\phi_{NGD}(\omega) + \phi_{PGD}(\omega). \tag{11}$$

By taking into account the GD definition of Equation (8), the GD of the proposed PGD-NGD PS can be approximated as:

$$GD_{PS}(\omega) \approx -\frac{\partial\left[2\phi_{NGD}(\omega) + \phi_{PGD}(\omega)\right]}{\partial\omega}. \tag{12}$$

This relation implies implicitly that:

$$GD_{PS}(\omega) \approx 2GD_{NGD}(\omega) + GD_{PGD}(\omega). \tag{13}$$

The analysis of the PS can be preceded by the unfamiliar BP NGD function.

### 2.4. BP PGD and NGD Analyses

The BP NGD analysis is necessary before the elaboration of the independent frequency PS under study. The main parameters associated with the PS analytical expression are elaborated in the present subsection. Accordingly, we assume that the block diagram of Fig. 1(b) behaves as an NGD function. Therefore, the corresponding GD response is characterized by the cut-off frequencies $\omega_a = 2\pi f_a$ and $\omega_b = 2\pi f_b$ with $\omega_a < \omega_b$, which are defined by:

$$GD_{NGD}(\omega_a) = GD_{NGD}(\omega_b) = 0. \tag{14}$$

The associated NGD bandwidth including the NGD center-frequency, $\omega_n = 2\pi f_n$, and value are respectively:

$$BW = \omega_b - \omega_a, \tag{15}$$

$$GD_{NGD}(\omega_a \leq \omega \leq \omega_b) = GD_n < 0. \tag{16}$$

Opposite to the NGD GD response, the PGD can be synthesized as follows. In an ideal aspect, the PGD diagram proposed in Fig. 1(a) can be characterized by the simplified expression:

$$GD_{PGD}(\omega_a \leq \omega \leq \omega_b) = GD_p > 0. \tag{17}$$

These definitions of parameters will be used in the rest of the paper to qualify the performance of the NGD circuit and the PS under study.

### 2.5. Analytical Formulation of the Independent-Frequency Phase Response of PGD-NGD PS

Figure 2 illustrates the expected ideal responses of phase and GD of the proposed PGD-NGD circuit. According to the GD definition given by Equation (8), we have the corresponding phase shifts plotted in Fig. 2(a):

$$\begin{cases} \phi_{PGD}(\omega_a \leq \omega \leq \omega_b) = GD_p\omega + \phi_p \\ \phi_{NGD}(\omega_a \leq \omega \leq \omega_b) = GD_n\omega + \phi_n \end{cases}. \tag{18}$$

Substituting the expressions of phase defined in Equation (13), this last equation becomes:

$$\phi_{PS}(\omega) \approx (GD_p + 2GD_n)\omega + \phi_p + 2\phi_n. \tag{19}$$

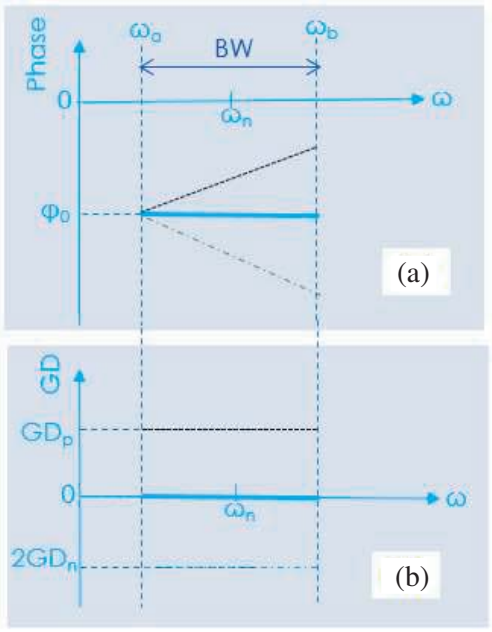


**Figure 2.** Ideal diagrams of (a) transmission phase and (b) GD responses.

Knowing the GD definition of Equation (8), the hypothesis of the independent-frequency phase shift corresponds analytically to:

$$GD_{PS}(\omega) = 0. \tag{20}$$

By considering Equation (13), this last equation implies that:

$$GD_p = -2GD_n. \tag{21}$$

Consequently, the PS phase introduced by Equation (19) is simplified as:

$$\phi_{PS}(\omega) = \phi_p + 2\phi_n = \phi_0. \tag{22}$$

This analytical demonstration explains the principle of independent frequency PS with the ideal response depicted in Fig. 2(b).

To implement this PS, the design with LCL-circuit as PGD and RLC-series resonant network circuit as NGD will be developed in the next subsection.

## 3. THEORY OF THE LCL AND NGD PS CIRCUIT

The present subsection describes the analytical investigation of LCL- and BP NGD-cells constituting the proposed independent frequency PS.

### 3.1. Modelling of the BP NGD Cell

Figure 3 shows the scheme of the BP NGD cell under study. The $S$-matrix model of this cell is composed of the coefficients expressed as:

$$S_{11NGD}(s) = \frac{-R_0Cs}{2LCs^2 + C(2R + R_0)s + 2}, \tag{23}$$

$$S_{21NGD}(s) = \frac{2\left[LCs^2 + RCs + 1\right]}{2LCs^2 + C(2R + R_0)s + 2}. \tag{24}$$

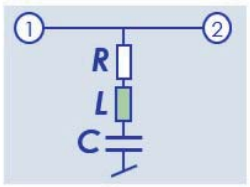


**Figure 3.** BP NGD cell.

The NGD analysis shows that the NGD center frequency and value, $GD_n = GD_{NGD}(\omega_n)$, of this cell can be expressed as:

$$\omega_n = \frac{1}{\sqrt{LC}}, \tag{25}$$

$$GD_n = \frac{-2R_0L}{R(R_0+2R)}. \tag{26}$$

The transmission and reflection coefficients at the NGD center frequency are given by:

$$S_{11NGD}(\omega_n) = \frac{R_0}{R_0+2R}, \tag{27}$$

$$S_{21NGD}(\omega_n) = \frac{2R}{R_0+2R}. \tag{28}$$

### 3.2. Modelling of the LCL-Network Based PGD Cell

Figure 4 depicts the LCL-cell representing the PGD circuit. This T-cell is composed of series inductance, $L_0$, and parallel capacitance, $C_0$. From the impedance matrix we can demonstrate the $S$-parameter model of this PCG circuit. The reflection and transmission coefficients of this PGD cell are expressed as:

$$S_{11PGD}(s) = \frac{s\left(L_0^2C_0s^2 - R_0^2C_0 + 2L_0\right)}{\left(R_0+L_0^s\right)\left(L_0C_0s^2 + R_0C_0s + 2\right)}, \tag{29}$$

$$S_{21PGD}(s) = \frac{2R_0}{\left(R_0+L_0s\right)\left(L_0C_0s^2 + R_0C_0s + 2\right)}. \tag{30}$$

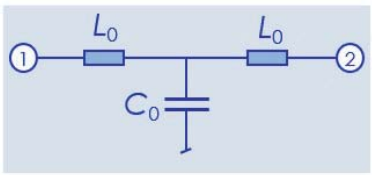


**Figure 4.** PGD LCL-based cell.

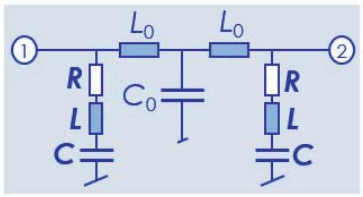


**Figure 5.** PS circuit constituted by LCL-NGD hybrid cell.

### 3.3. PS Circuit Analysis and Design Equation

Figure 5 introduces the PS cell constituted by combined NGD and PGD circuits. The insertion of the two NGD networks in the access port can ensure the matching condition.

By considering the transfer matrix and $ABCD$-to-$S$ matrix transform, we have the analytical model of our LCL-NGD PS written as:

$$S_{11PS}(s) = \frac{n_7s^7 + n_6s^6 + n_5s^5 + n_4s^4 + n_3s^3 + n_2s^2 + n_1s + n_0}{d_7s^7 + d_6s^6 + d_5s^5 + d_4s^4 + d_3s^3 + d_2s^2 + d_1s + d_0}, \tag{31}$$

$$S_{21PS}(s) = \frac{2R_0\left[LC^2s^3(Ls+2R)+C(2L+R^2C)s^2+2RCs+1\right]}{d_7s^7+d_6s^6+d_5s^5+d_4s^4+d_3s^3+d_2s^2+d_1s+d_0}, \tag{32}$$

with

$$\begin{cases} n_7 = L_0^2C_0L^2C^2 \\ n_6 = 2RL_0^2C_0LC^2 \\ n_5 = C\left[L^2(2L_0-R_0C_0)-2L_0C_0L(CR_0^2-L_0)+L_0^2C_0C(R^2-R_0^2)\right] \\ n_4 = 2RC\left[LC(2L_0-R_0^2C_0)+L_0C_0(L_0-R_0^2C_0)\right] \\ n_3 = 2R^2C^2(L_0-R_0^2C_0)+L_0\left[C_0(L_0-2R_0^2C)-2R_0^2C^2\right] \\ n_2 = 2RC\left[2L_0-R_0^2(C+C_0)\right] \\ n_1 = 2R\left[2L_0C-R_0^2C(C+C_0)\right] \\ n_0 = 2L_0-R_0^2(2C+C_0) \end{cases}, \tag{33}$$

$$\begin{cases} d_7 = L_0^2C_0L^2C^2 \\ d_6 = 2L_0C_0LC^2\left[L_0R+R_0(L+L_0)\right] \\ d_5 = C\left[L^2(2L_0+R_0C_0^2)+2L_0C_0LC(CR_0^2+L_0+2RR_0C)+L_0^2C_0C^2(R+R_0)\right] \\ d_4 = 2C\left[R_0CL^2+2L(R(R_0^2C_0C+2L_0C)+2R_0L_0(2C+C_0))+L_0C_0C(R+R_0)(L_0+RR_0C)\right] \\ d_3 = \left\{\begin{array}{l} 2LC\left[2R_0RC+2L_0+R_0^2(C+C_0)\right]+R^2C^2(2L_0+R_0^2C_0)+4RR_0L_0C(C+C_0) \\ +L_0\left[L_0C_0+2R_0^2C(C_0+C)\right] \end{array}\right\} \\ d_2 = 2\left[R_0C^2R^2+R(2L_0C+R_0^2C(C+C_0))+R_0L_0(2C+C_0)\right] \\ d_1 = 2L_0+4R_0RC+R_0^2(2C+C_0) \\ d_0 = 2R_0 \end{cases}. \tag{34}$$

The main specifications of our NGD PS to be defined before the design are:

- Center frequency, $f_n = \omega_n/(2\pi)$,
- The level of the input and output matching corresponding to the reflection parameter which is a real positive value denoted $a < 1$,
- And the phase shift which is a real value, $\phi_0$.

From this model, we can determine the magnitude and shift at the NGD center frequency:

$$S_{11NGD}(\omega_n) = a, \tag{35}$$

$$GD_{PS}(\omega_n) = 0, \tag{36}$$

$$\phi_{PS}(\omega_n) = \phi_0, \tag{37}$$

where $a$ denotes the total GD annihilation, and $\omega_n$ denotes the center frequency. The parameters $R$, $L$, and $C$ can be derived from the NGD specifications of matching level as:

$$R = \frac{R_0(1-a)}{2a}, \tag{38}$$

$$L = \frac{RL_0(2R+R_0)}{R_0^2}, \tag{39}$$

$$C = \frac{1}{L\omega_n^2}. \tag{40}$$

Then, we can derive the synthesis design equation of the PGD circuit. The circuit parameters are established from the equalization of the PGD and NGD GD, $GD_{PGD}(\omega_n) + GD_{NGD}(\omega_n) = 0 \Rightarrow GD_{PGD}(\omega_n) + GD_n = 0$, and the desired phase shift at the chosen center frequency based on Equation (37). Therefore, we have the synthesis formulas expressed as:

$$C_0 = \frac{\tan(\phi_0)}{R_0\omega_n\sqrt{1+\tan^2(\phi_0)}}, \tag{41}$$

$$L_0 = \frac{(1-C_0R_0\omega_n)\left(1+\sqrt{1+C_0R_0\omega_n}\right)}{C_0\omega_n^2}. \tag{42}$$

To confirm the feasibility of the BP NGD function based innovative PS, a validation study is proposed in the following section.

## 4. VALIDATION RESULTS

To validate the developed design method of the independent frequency LCL-NGD PS, a proof-of-concept (POC) was designed and simulated. The design and simulations were performed in the ADS® environment of microwave circuit simulator commercial tool from Keysight Technologies®. The following subsections describe the obtained results.

### 4.1. Design Description of the POC LCL-NGD Circuit

The present validation is based on the design of LCL-NGD PS with the previously established theoretical model. As the initial step of the practical study, we need to define the targeted objectives of the LCL-NGD PS design. In the present case of an investigation, the desired specifications are given in Table 1. These values of specifications were arbitrarily chosen to verify the effectiveness of the LCL-NGD PS design, but it can also be applied to various cases of RF and microwave transceiver in the future.

**Table 1.** Desired specifications of the PGD-NGD PS.

| Description | Center frequency | Phase value | Reflection coefficient | Transmission coefficient |
|---|---|---|---|---|
| Parameter | $f_n$ | $\phi_n$ | $S_{11n}$ | $S_{21n}$ |
| Value | 1.2 GHz | $-120°$ | $-15$ dB | $-3$ dB |

Figures 6(a), 6(b), and 6(c) represent the schematics of the designed PGD, NGD, and LCL-NGD PS circuits, respectively. These schematics, which are implemented in the ADS®environment, are composed of lumped RLC-components. The synthesized components and approximated simulated values are depicted in Table 2. The equivalent $S$-parameter models of NGD, LCL, and LCL-NGD PS

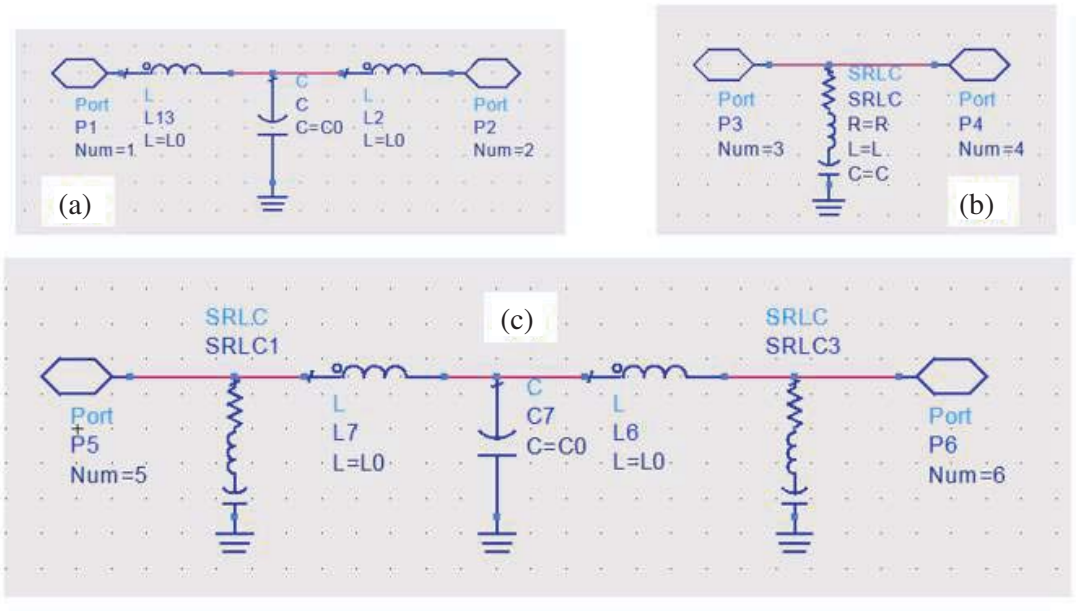


**Figure 6.** Schematics of (a) LCL-PGD, (b) NGD and (c) LCL-NGD PS circuits designed in the ADS® environment.

**Table 2.** Parameters of the LCL-NGD PS POC.

| Circuit | Type | Calculated value | Approximated simulated parameters |
|---|---|---|---|
| PGD | Inductor | $L_0 = 11.03\,\text{nH}$ | $L_0 = 11\,\text{nH}$ |
| | Capacitor | $C_0 = 2.205\,\text{pF}$ | $C_0 = 2.2\,\text{pF}$ |
| NGD | Resistor | $R = 108.114\,\Omega$ | $R = 108\,\Omega$ |
| | Inductor | $L = 75.4\,\text{nH}$ | $L = 75\,\text{nH}$ |
| | Capacitor | $C = 0.22\,\text{pF}$ | $C = 0.22\,\text{pF}$ |

circuits were calculated with MATLAB® based on formulas of the analytical expressions established in:

- Equations (23) and (24) for the NGD circuit,
- Equations (29) and (30) for the LCL PGD circuit,
- Equations (31) and (32) for the innovative LCL-NGD PS circuit POC.

After the $S$-parameter simulations of these three circuits, the comparative validation results are discussed in the following subsections.

### 4.2. Simulated and Modeled PS Performances

The validation of the previously designed PS was done with $S$-parameter frequency domain analysis from 1.1 GHz to 1.4 GHz. After computations, we obtained the LCL-NGD PS, BP NGD circuit PS, and LCL PGD circuit PS, which are shown respectively in Fig. 7(a), Fig. 7(b), and Fig. 7(c). The simulated

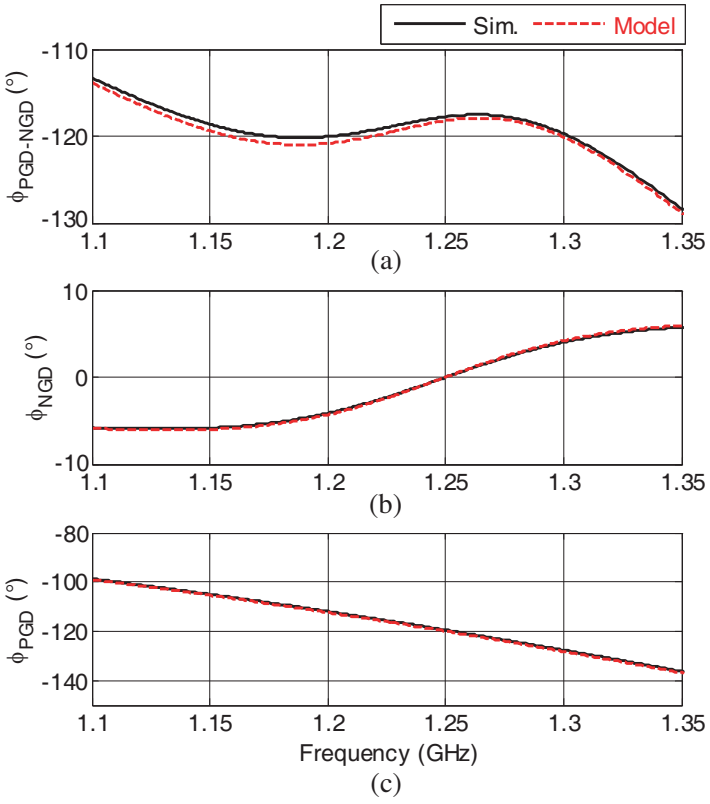


**Figure 7.** Comparison of simulated and modeled (a) phase shift, (b) $S_{21}$, and (c) $S_{11}$ of the LCL-NGD PS circuit shown in Fig. 5(c).

("Sim.") and modeled ("Model") results are displayed respectively in black solid and red dashed lines. We would like to emphasize that the NGD circuit is needed to have the frequency independent phase shift (plotted in Fig. 7(a)) from frequencies $f_1$ and $f_2$ under the flatness relative tolerance. Without NGD function, we have a classical negative slop phase shift of PGD shown in Fig. 7(a). The corresponding GDs, transmission coefficients, and reflection coefficients of the three circuits are shown in Fig. 8, Fig. 9, and Fig. 10, respectively. As expected, a very good correlation between the analytical model and ADS® simulation is confirmed.

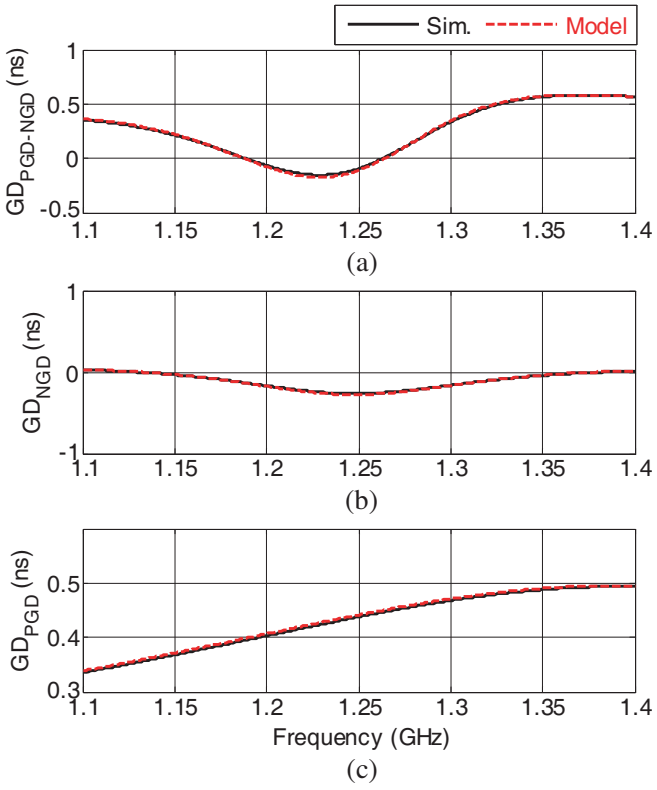


**Figure 8.** Comparison of simulated and modeled phase shift from the (a) PS, (b) NGD, and (c) PGD circuits.

**Table 3.** Performances of the LCL-NGD PS POC.

| Circuit | Parameters | Model | Simulation |
|---|---|---|---|
| PS | $\phi_0 = \phi_{PS}(f_0)$ | $-120.05°$ | $-120.8°$ |
| | $f_1$ | 1.109 GHz | 1.114 GHz |
| | $f_2$ | 1.331 GHz | 1.333 GHz |
| | $\Delta f$ | 222 MHz | 219 MHz |
| | $\Delta f/f_0$ | 18.5% | 18.25% |
| | $S_{11PS}(f_0)$ | $-15.9$ dB | $-16.15$ dB |
| | $S_{21PS}(f_0)$ | $-3.77$ dB | $-3.72$ dB |
| | $\Delta S_{21}$ | 1.48 dB | 1.42 dB |
| NGD | $GD_n$ | $-0.174$ ns | $-0.168$ ns |
| | $S_{11NGD}(f_0)$ | $-14.89$ dB | $-15.06$ dB |
| | $S_{21NGD}(f_0)$ | $-1.58$ dB | $-1.55$ dB |

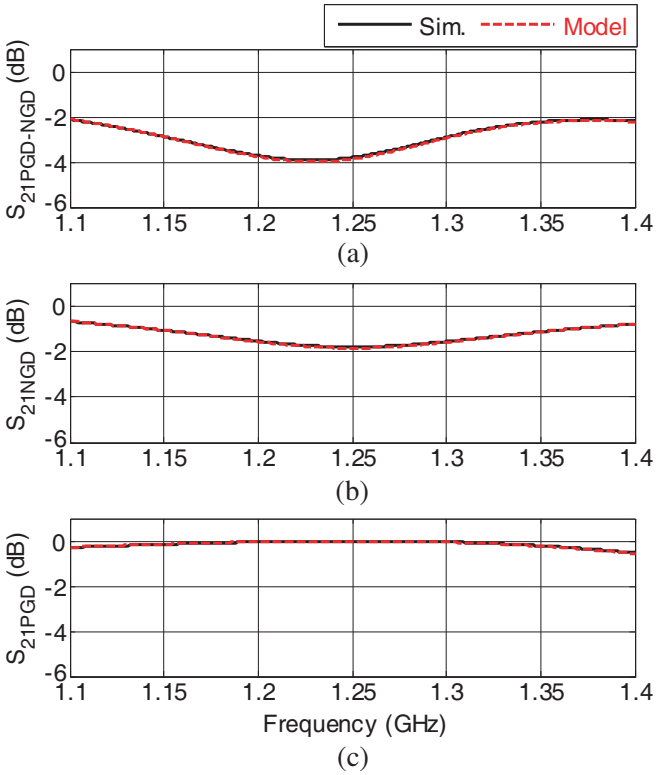


**Figure 9.** Comparison of simulated and modeled $S_{21}$ from the (a) PS, (b) NGD, and (c) PGD circuits.

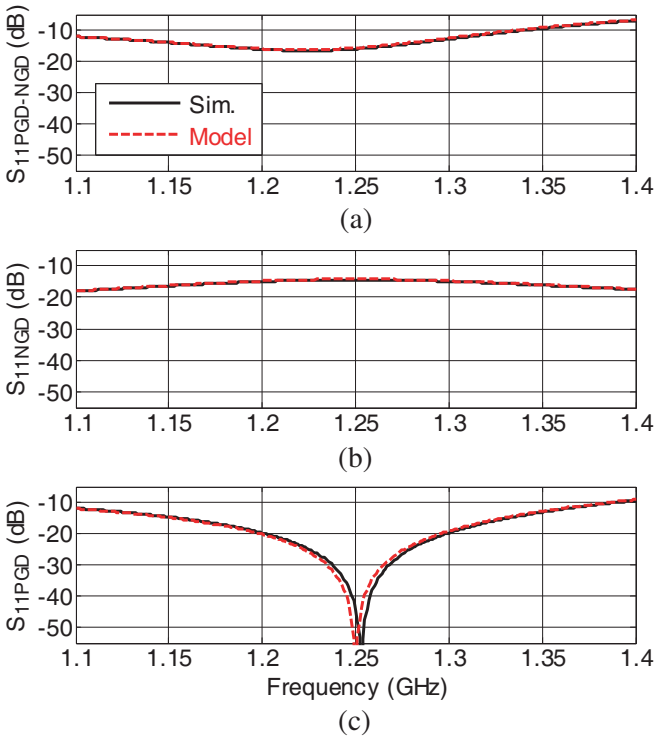


**Figure 10.** Comparison of simulated and modeled $S_{11}$ from the (a) PS, (b) NGD, and (c) PGD circuits.

We can underline that the LCL-NGD PS POC presents an outstanding phase shift flatness. We evaluate a flatness of the phase value with the accuracy $\phi_{PS} = -120° \pm 5°$ with center frequency $f_0 = 1.2\,\text{GHz}$. The bandwidth of the LCL-NGD PS is defined by $\Delta f = f_2 - f_1$, with frequency limits, $f_1$, and $f_2$, verifying:

$$\begin{cases} \phi_{PS}(f_1) = 0.95\phi_0 \\ \phi_{PS}(f_2) = 1.05\phi_0 \end{cases}. \tag{43}$$

More importantly, the flatness of the transmission parameter is evaluated by:

$$\Delta S_{21} = \max\left[S_{21\,\text{dB}}(f_1) - S_{21\,\text{dB}}(f_0), S_{21\,\text{dB}}(f_2) - S_{21\,\text{dB}}(f_0)\right]. \tag{44}$$

The transmission coefficient is about $S_{21PS}(f_n) = -2.6\,\text{dB} \pm 1.2\,\text{dB}$, and the reflection coefficient is kept better than $-15\,\text{dB}$. The independent frequency aspect of the phase response is confirmed with the performances summarized in Table 3. Then, it is also indicated in the table that the NGD circuit specifications are also assessed with about $-0.1\,\text{ns}$ NGD value.

### 4.3. Sensitivity Analysis of the LCL-NGD PS versus the NGD Circuit Parameters

To illustrate the sensitivity of the LCL-NGD PS, parametric analyses of the NGD circuit elements were performed. Each component, $R$, $L$, and $C$, was assumed with relative variations about $\pm 5\%$. The following paragraphs describe the obtained results.

#### *4.3.1. Effect of NGD Circuit Resistance Variation*

Figure 11 displays the mappings of the LCL-NGD PS value, $S_{21}$ and $S_{11}$ responses versus frequency and components $R \pm 5\%$. The mapping shown by Fig. 11(a) presents the variation of the LCL-NGD PS phase shift, which shows that the phase value varies sensitively to the NGD circuit resistance variations. The same aspect is illustrated by the mapping of the transmission coefficient shown in Fig. 11(b). However, the LCL-NGD PS central frequency remains constant. Table 4 addresses the variation of the phase, transmission coefficient, insertion loss flatness, and reflection coefficient. It can be underlined that the

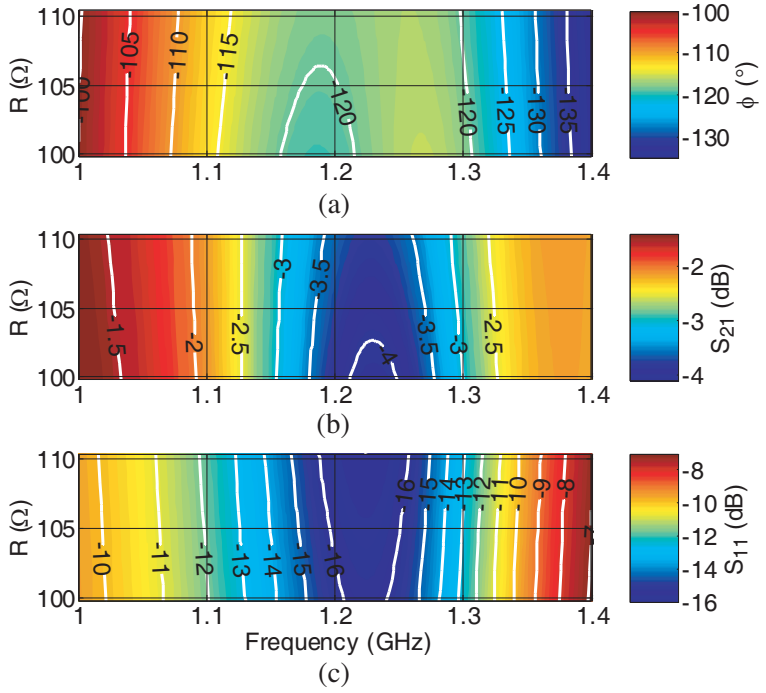


**Figure 11.** Mapping of (a) phase shift, (b) $S_{21}$, and (c) $S_{11}$ versus (frequency, $R$).

**Table 4.** Variations of the LCL-NGD PS performances in the function of the NGD circuit resistance variation effect.

| $R(\Omega)$ | $\phi_{PS}(f_0)$ (°) | $\Delta f$ (GHz) | $S_{21n}$ (dB) | $\Delta S_{21}$ (dB) | $S_{11n}$ (dB) |
|---|---|---|---|---|---|
| 99.883 | −120.795 | 0.226 | −3.853 | 1.62 | −15.809 |
| 101.9858 | −120.486 | 0.224 | −3.799 | 1.56 | −15.951 |
| 104.0886 | −120.191 | 0.222 | −3.746 | 1.474 | −16.089 |
| 106.1914 | −119.91 | 0.218 | −3.694 | 1.39 | −16.223 |
| 108.2942 | −119.642 | 0.216 | −3.643 | 1.308 | −16.353 |
| 110.397 | −119.387 | 0.21 | −3.594 | 1.222 | −16.479 |

reflection coefficient remains widely better than −10 dB as depicted in Fig. 11(c). However, the phase shift, $\phi_{PS}(f_0)$, presents a variation amplitude about 1.41°.

### *4.3.2. Effect of NGD Circuit Inductance Variation*

Figure 12 depicts the mapping of the LCL-NGD PS versus frequency and $L$ under ±5% relative variation. It can be found in Fig. 12(a) and Fig. 12(b) that the phase value and the transmission coefficient vary sensitively to the three-component variations. In addition, the LCL-NGD PS central frequency is significantly sensitive to the inductor variation. Table 5 quantifies the LCL-NGD PS performance variations in function of the NGD circuit inductance. In this case, the phase shift at the central frequency, $\phi_{PS}(f_0)$, shows a variation with an amplitude about 9°. Then, the insertion loss variation is about 1.05 dB with reflection loss widely better than 10 dB in the whole range of the inductance variation.

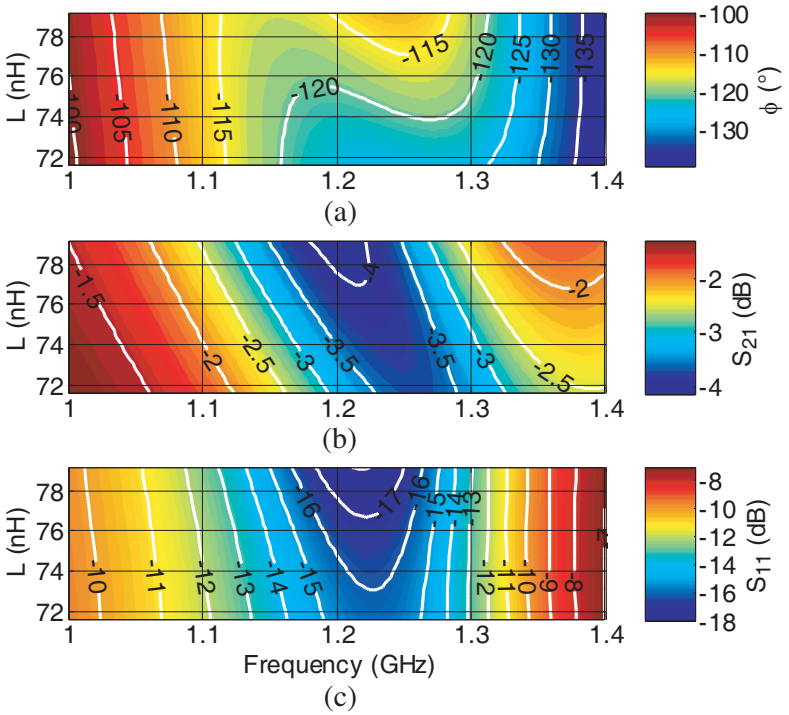


**Figure 12.** Mapping of (a) phase shift, (b) $S_{21}$, and (c) $S_{11}$ versus (frequency, $L$).

**Table 5.** Variations of the LCL-NGD PS performances in the function of the NGD circuit inductance variation effect.

| $L$(nH) | $\phi_0$ (°) | $\Delta f$ (GHz) | $S_{21n}$ (dB) | $\Delta S_{21}$ (dB) | $S_{11n}$ (dB) |
|---|---|---|---|---|---|
| 71.63 | −123.425 | 0.194 | −3.102 | 1.62 | −15.306 |
| 73.138 | −122.34 | 0.21 | −3.358 | 1.56 | −15.576 |
| 74.646 | −120.905 | 0.218 | −3.604 | 1.474 | −15.937 |
| 76.154 | −119.102 | 0.22 | −3.828 | 1.39 | −16.405 |
| 77.662 | −116.95 | 0.062 | −4.011 | 1.308 | −16.995 |
| 79.17 | −114.507 | 0.222 | −4.138 | 1.222 | −17.722 |

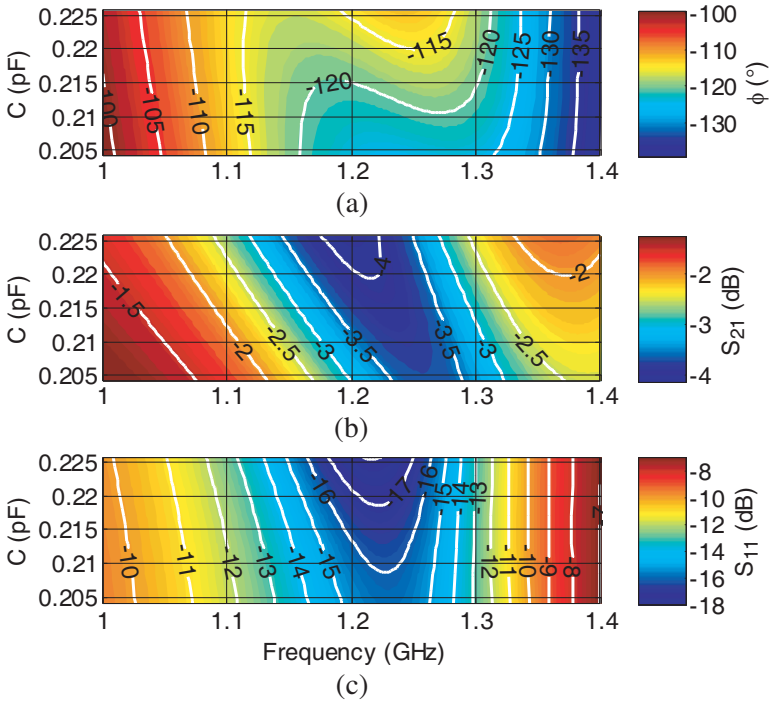


**Figure 13.** Mapping of (a) phase shift, (b) $S_{21}$, and (c) $S_{11}$ versus (frequency, $C$).

**Table 6.** Variations of the LCL-NGD PS performances in the function of the NGD circuit capacitor variation effect.

| $C$ (pF) | $\phi_0$ (°) | $\Delta f$ (GHz) | $S_{21n}$ (dB) | $\Delta S_{21}$ (dB) | $S_{11n}$ (dB) |
|---|---|---|---|---|---|
| 0.20425 | −123.733 | 0.194 | −3.011 | 1.152 | −15.229 |
| 0.20855 | −122.558 | 0.21 | −3.312 | 1.302 | −15.521 |
| 0.21285 | −120.982 | 0.218 | −3.593 | 1.4 | −15.918 |
| 0.21715 | −119.028 | 0.22 | −3.835 | 1.556 | −16.425 |
| 0.22145 | −116.764 | 0.064 | −4.024 | 1.925 | −17.048 |
| 0.22575 | −114.293 | 0.22 | −4.145 | 2.189 | −17.789 |

*4.3.3. Effect of NGD Circuit Capacitor Variation*

Figure 13 depicts the mappings of the LCL-NGD PS performances versus frequency and the NGD circuit capacitor under ±5% relative variation, respectively. Table 6 summarizes the LCL-NGD PS phase value, shift of the center frequency, transmission, and reflection coefficients. We can see in Fig. 13(a) that the phase value varies sensitively to the capacitance variations with about 10° amplitude. Similar to the previous case of the study, the LCL-NGD PS central frequency is particularly sensitive to capacitor fluctuation. As seen in Fig. 13(b), the transmission coefficient at the central frequency is shifted by less than 1.2 dB. However, the PS remains well matched with a reflection coefficient better than −10 dB as illustrated in Fig. 13(c).

## 5. CONCLUSION

An innovative design method of passive NGD PS operating independently of the frequency is investigated. The PS is topologically imagined from the cascade combination of PGD and NGD circuits. The topological implementation principle of the proposed PS is described with analytical formulations of the phase value. It is explained how the PGD-NGD PS is ideally susceptible to operate with constant phase or zero GD value. The principle is based on the exploitation of the BP NGD function.

The core of the PGD-NGD PS circuit is based on the combination of an RLC-series network as an NGD circuit at the input and out ports and an LCL T-cell as a PGD circuit. The innovative theoretical study of the PS is illustrated with $S$-matrix modeling. The analytical model of the NGD, PGD, and PS circuit equivalent $S$-parameters is established. Moreover, the design equations enabling the determination of each component of the PS to the given specifications are carefully formulated.

The validity of the proposed LCL-NGD PS design is verified with a POC lumped circuit. The obtained results of the calculated and simulated phases, transmission, and reflection coefficients of the LCL-NGD PS POC are in very good correlation. Furthermore, the PS performances are also investigated with mapping cartographies versus frequency and components $R$, $L$, and $C$, respectively. Therefore, the phase value varies sensitively nearly about ±5% to the relative variations of the NGD circuit components. As a result, the PS central frequency is only sensitive to the inductor and capacitor.

In the continuation of the present study, the fabrication and test of the PS in CMOS technology are in progress for the improvement of the transceiver architecture with the possibility to overcome the challenging function as the implementation of Hilbert filter.

## ACKNOWLEDGMENT

This work was supported by the Deanship of Scientific Research at Prince Sattam bin Abdulaziz University, Saudi Arabia. This research work was also supported in part by NSFC under Grant 61971230, and in part by Jiangsu Specially Appointed Professor program and Six Major Talents Summit of Jiangsu Province (2019-DZXX-022) and in part by the Startup Foundation for Introducing Talent of NUIST, in part by the Postgraduate Research & Practice Innovation Program of Jiangsu Province under Grant KYCX20_0966.

## REFERENCES

1. Macke, B. and B. Ségard, "Propagation of light-pulses at a negative group-velocity," *Eur. Phys. J. D*, Vol. 23, 125–141, 2003.
2. Munday, J. N. and W. M. Robertson, "Observation of negative group delays within a coaxial photonic crystal using an impulse response method," *Optics Communications*, Vol. 273, No. 1, 32–36, 2007.
3. Eleftheriades, G. V., O. Siddiqui, and A. K. Iyer, "Transmission line for negative refractive index media and associated implementations without excess resonators," *IEEE Microw. Wireless Compon. Lett.*, Vol. 13, No. 2, 51–53, Feb. 2003.

4. Siddiqui, O. F., M. Mojahedi and G. V. Eleftheriades, "Periodically loaded transmission line with effective negative refractive index and negative group velocity," *IEEE Trans. Antennas Propagat.*, Vol. 51, No. 10, 2619–2625, Oct. 2003.
5. Markley, L. and G. V. Eleftheriades, "Quad-band negative-refractive-index transmission-line unit cell with reduced group delay," *Electronics Letters*, Vol. 46, No. 17, 1206–1208, Aug. 2010.
6. Monti, G. and L. Tarricone, "Negative group velocity in a split ring resonator-coupled microstrip line," *Progress In Electromagnetics Research*, Vol. 94, 33–47, 2009.
7. Mitchell, M. W. and R. Y. Chiao, "Negative group delay and "fronts" in a causal system: An experiment with very low-frequency bandpass amplifiers," *Phys. Lett. A*, Vol. 230, No. 3–4, 133–138, Jun. 1997.
8. Munday, J. N. and R. H. Henderson, "Superluminal time advance of a complex audio signal," *Appl. Phys. Lett.*, Vol. 85, No. 3, 503–504, Jul. 2004.
9. Wan, F., J. Wang, B. Ravelo, J. Ge, and B. Li, "Time-domain experimentation of NGD active RC-network cell," *IEEE Trans. Circuits and Systems II: Express Briefs*, Vol. 66, No. 4, 562–566, Apr. 2019.
10. Ahn, K.-P., R. Ishikawa, A. Saitou, and K. Honjo, "Synthesis for negative group delay circuits using distributed and second-order RC circuit configurations," *IEICE Trans. on Electronics*, Vol. E92-C, No. 9, 1176–1181, 2009.
11. Kandic, M. and G. E. Bridges, "Asymptotic limits of negative group delay in active resonator-based distributed circuits," *IEEE Transactions on Circuits and Systems I: Regular Papers*, Vol. 58, No. 8, 1727–1735, Aug. 2011.
12. Zhang, T., R. Xu, and C. M. Wu, "Unconditionally stable non-foster element using active transversal-filter-based negative group delay circuit," *IEEE Microw. Wireless Compon. Lett.*, Vol. 27, No. 10, 921–923, Oct. 2017.
13. Ravelo, B., "Investigation on microwave negative group delay circuit," *Electromagnetics*, Vol. 31, No. 8, 537–549, Nov. 2011.
14. Wu, C.-T. M. and T. Itoh, "Maximally flat negative group delay circuit: A microwave transversal filter approach," *IEEE Trans. on Microwave Theory and Techniques*, Vol. 62, No. 6, 1330–1342, Jun. 2014.
15. Liu, G. and J. Xu, "Compact transmission-type negative group delay circuit with low attenuation," *Electronics Letters*, Vol. 53, No. 7, 476–478, Mar. 2017.
16. Chaudhary, G. and Y. Jeong, "Tunable center frequency negative group delay filter using a coupling matrix approach," *IEEE Microwave Wireless Component Letters*, Vol. 27, No. 1, 37–39, 2017.
17. Shao, T., S. Fang, Z. Wang, and H. Liu, "A compact dual-band negative group delay microwave circuit," *Radio Engineering*, Vol. 27, No. 4, 1070–1076, Dec. 2018.
18. Ravelo, B., "Similitude between the NGD function and filter gain behaviours," *Int. J. Circ. Theor. Appl.*, Vol. 42, No. 10, 1016–1032, Oct. 2014.
19. Broomfield, C. D. and J. K. A. Everard, "Broadband negative group delay networks for compensation of oscillators, filters and communication systems," *Electron. Lett.*, Vol. 36, No. 23, 1931–1933, Nov. 2000.
20. Choi, H., Y. Jeong, C. D. Kim, and J. S. Kenney, "Efficiency enhancement of feedforward amplifiers by employing a negative group delay circuit," *IEEE Trans. Microw. Theory Tech.*, Vol. 58, No. 5, 1116–1125, May 2010.
21. Choi, H., Y. Jeong, C. D. Kim, and J. S. Kenney, "Bandwidth enhancement of an analog feedback amplifier by employing a negative group delay circuit," *Progress In Electromagnetics Research*, Vol. 105, 253–272, 2010.
22. Mirzaei, H. and G. V. Eleftheriades, "Realizing non-Foster reactive elements using negative-group-delay networks," *IEEE Trans. Microw. Theory Techn.*, Vol. 61, No. 12, 4322–4332, Dec. 2013.
23. Mortazawi, A. and W. Alomar, "Negative group delay circuit," United States Patent Application US20160093958, Mar. 2016.

24. Zhu, M. and C.-T. M. Wu, "Reconfigurable series feed network for squint-free antenna beamforming using distributed amplifier-based negative group delay circuit," *Proc. 2019 49th European Microwave Conference (EuMC)*, 256–259, Paris, France, Oct. 1–3, 2019.
25. Ravelo, B., "Distributed NGD active circuit for RF-microwave communication," *International Journal of Electronics and Communications (AEÜ)/Int. J. Electron. Commun.*, Vol. 68, No. 4, 282–290, Apr. 2014.
26. Ravelo, B., S. Lalléchère, A. Thakur, A. Saini, and P. Thakur, "Theory and circuit modelling of baseband and modulated signal delay compensations with low- and band-pass NGD effects," *Int. J. Electron. Commun.*, Vol. 70, No. 9, 1122–1127, Sept. 2016.
27. Shao, T., Z. Wang, S. Fang, H. Liu, and Z. N. Chen, "A group-delay-compensation admittance inverter for full-passband self-equalization of linear-phase band-pass filter," *Int. J. Electron. Commun.*, Vol. 123, No. 153297, 1–6, 2020.